ORIGINAL RESEARCH

P. de Graaf
P.J.W. Pouwels
F. Rodjan
A.C. Moll
S.M. Imhof
D.L. Knol
E. Sanchez
P. van der Valk
J.A. Castelijns

Single-Shot Turbo Spin-Echo Diffusion-Weighted Imaging for Retinoblastoma: Initial Experience

BACKGROUND AND PURPOSE: Retinoblastoma may exhibit variable hyperintensities on DWI, resulting in different values in the ADC maps, depending on their histology and cellularity. However, EP-based DWI has susceptibility artifacts and image distortions, which make DWI of the orbit a challenging technique. The aim of this study was to investigate the feasibility of single-shot turbo spin-echo (HASTE) DWI in the evaluation of children with retinoblastoma and to assess the value of ADC maps in differentiating viable and necrotic tumor tissue.

MATERIALS AND METHODS: Two radiologists assessed conventional MR images, DWI, and ADC maps of 17 patients with retinoblastoma ($n = 17$ eyes). Non-EP DWI was performed by using a HASTE sequence with b-values of 0 and 1000 s/mm^2. ADC values were measured for enhancing and nonenhancing tumor tissue. ADC maps were compared with histopathologic findings regarding tumor differentiation and viability.

RESULTS: On DWI, vital tumor tissue showed hyperintensity with negligible intensity of surrounding vitreous. The difference in mean (range) ADC values between enhancing ($1.03\ [0.72–1.22] \times 10^{-3}$ mm^2 s^{-1}) and nonenhancing ($1.47\ [0.99–1.80] \times 10^{-3}$ mm^2 s^{-1}) parts of retinoblastoma was statistically significant ($P < .0005$). Nonenhancing tumor parts showed a significantly lower ADC compared with vitreous ($2.67\ [2.24–3.20] \times 10^{-3}$ mm^2 s^{-1}) ($P < .0005$) and subretinal fluid ($2.20\ [1.76–2.96] \times 10^{-3}$ mm^2 s^{-1}) ($P < .0005$). Histopathologically, low ADC values (enhancing tumor part) correlated to viable tumor tissue, whereas intermediate ADC values (nonenhancing tumor parts) correlated to necrotic tumor tissue.

CONCLUSIONS: HASTE DWI allowed adequate characterization of retinoblastoma, and ADC is a helpful tool to differentiate viable and necrotic tumor tissue and might be valuable in monitoring the response to eye-preserving therapies.

ABBREVIATIONS: EP = echo-planar; HASTE = half-Fourier acquired single-shot turbo spin-echo; SI = signal intensity

Although the diagnosis of retinoblastoma is usually made by funduscopy and sonography, ocular MR imaging plays a confirmatory role in the diagnostic process and a crucial role in staging local disease extent and detecting midline intracranial masses and metastases.[1-3] When clinical diagnosis is uncertain, MR imaging helps to characterize and differentiate benign and malignant simulating lesions, to definitively rule out a retinoblastoma.[4] However, in some cases, morphologic information and tumor characteristics on conventional MR images are not sufficient to confirm the diagnosis. Despite the increasing use of MR imaging in ocular oncology, the main cause of erroneous diagnosis in the work-up of children with leukocoria is still (advanced stage) Coats disease, followed by persistent hyperplastic primary vitreous.[5] Therefore, a supplementary noninvasive diagnostic technique would be desirable.

With the expanding possibilities in nonoperative management of retinoblastoma, increasing numbers of patients will be treated with these eye-preserving therapies. However, at present no noninvasive markers are available that can reliably predict response to conservative therapy in retinoblastoma. Development of a sensitive MR imaging method that allows early prediction of treatment response might assist in future selection of the optimal therapeutic strategy for patients with retinoblastoma.

DWI is widely used in neuroimaging, particularly for the evaluation of acute cerebral stroke and intracranial tumors.[6,7] ADC measured by DWI has been proposed as the technique of choice for detection of early response to treatment in brain tumors and head and neck cancers.[8-10] DWI is based on the diffusion of water molecules in tissue, which depends on the attenuation of cell membranes. The technique detects abnormalities based on differences in tissue cellularity. Therefore, DWI enables the characterization of tissues on a microscopic level and uses a mechanism that is different from conventional MR imaging sequences that are based on T1 and T2 relaxation. An EP-based sequence is the traditional choice for DWI. EP sequences are very fast but are sensitive to susceptibility artifacts and image distortions, which are particularly present at air-tissue and bone-tissue interfaces. Therefore, DWI of the orbit is a challenging technique, especially by using an EP-

Received March 13, 2011; accepted after revision May 1.

From the Departments of Radiology (P.d.G., F.R., E.S., J.A.C.), Physics and Medical Technology (P.J.W.P.), Ophthalmology (A.C.M.), Pathology (P.v.d.V.), and Epidemiology and Biostatistics (D.L.K.), VU University Medical Center, Amsterdam, the Netherlands; and Department of Ophthalmology (S.M.I.), University Medical Center Utrecht, Utrecht, the Netherlands

Pim de Graaf, MD, is financially supported, in part, by grants from the ODAS Foundation, Delft, the Netherlands; ZonMw (Netherlands Organization for Health Research and Development), The Hague, the Netherlands; National Foundation for the Blind and Visually Impaired, Utrecht, the Netherlands; the Blindenhulp Foundation, The Hague, the Netherlands and the Dutch Eye Fund (grant 2004–23), Utrecht, the Netherlands.

Please address correspondence to Pim de Graaf, MD, VU University Medical Center, Department of Radiology, PO Box 7057, 1007 MB Amsterdam, the Netherlands; e-mail: p.degraaf@vumc.nl

Indicates open access to non-subscribers at www.ajnr.org

http://dx.doi.org/10.3174/ajnr.A2729

based diffusion sequence. Recently, first applications of EP DWI in the orbit enabled successful differentiation of malignant (lymphoid) lesions, benign lesions, and inflammatory conditions.[11-14]

In our study, we explored the potential of a non-EP DWI technique based on a HASTE sequence. Because the image acquisition is based on turbo spin-echo, it does not have image distortions and susceptibility artifacts present in EP-based techniques.[15] The acquisition time of HASTE DWI sequences is longer, but the absence of geometric distortion allows an adequate coregistration with conventional MR images. The use of a relatively high spatial resolution possibly allows the detection of small intraocular lesions.[16] However, to our knowledge, no data are available in the literature, neither on the value of non-EP DWI in the orbit nor on DWI in a series of patients with retinoblastoma.

The purpose of our study was to investigate the feasibility of HASTE DWI in the evaluation of children with retinoblastoma and to assess the value of ADC maps in differentiating viable and necrotic tumor tissue.

Materials and Methods

Patients

Consecutive patients referred to our hospital with leukocoria and a clinically suspected retinoblastoma were prospectively enrolled in the study from October 2008 to October 2010. Before MR imaging examinations, all patients underwent funduscopy and sonography under general anesthesia. Patients were included in the study if they met the following criteria: 1) having undergone pretreatment 1.5T contrast-enhanced MR imaging, including HASTE-DWI, which enabled adequate image interpretation; and 2) having undergone enucleation of the eye with retinoblastoma, without therapeutic interventions in the affected eye before enucleation. Eighteen of 24 patients met these inclusion criteria. However, 1 pathologic specimen could not be evaluated because the remainder of tumor tissue was too small for proper analysis, so this patient was excluded from the study. The final study population consisted of 17 patients with a mean age at MR imaging of 32 months (age range, 1–124 months), which included 5 (29%) girls and 12 (71%) boys. None of the 3 (18%) bilaterally affected patients underwent enucleation of both eyes. Thus, data obtained from 17 eyes could be evaluated. The right eye was enucleated in 9 (53%) and the left eye in 8 (47%) patients. The mean interval between MR imaging and enucleation was 7 days (range, 1–13 days). None of the patients showed a positive family history of retinoblastoma. This prospective study was conducted in accordance with recommendations of the local ethics committee, with waiver of informed consent.

Conventional MR Imaging

MR imaging with the patient under general anesthesia was performed with a 1.5T clinical MR imaging system (Sonata; Siemens, Erlangen, Germany) by using a standard quadrature head coil and a dedicated surface coil focused on the affected eye. The gradient strength of the magnet was 40 mT/m. The routine retinoblastoma MR imaging protocol included the use of transverse and sagittal spin-echo T1-weighted (TR, 370 ms; TE, 14 ms) and turbo spin-echo transverse T2-weighted (TR, 3460 ms; TE, 116 ms) MR images. Patients received 0.02 mmol/kg of body weight of gadolinium chelate (7 patients, gadopentetate dimeglumine, Magnevist; Schering, Berlin, Germany; and 10 patients, gadoterate dimeglumine, Dotarem; Guerbet, Roissy, Charles-de-gaulle Cedex; France). Postcontrast images were obtained in transverse and sagittal directions with spin-echo T1-weighted images (15 patients) and spin-echo fat-suppressed T1-weighted images (TR, 653 ms; TE, 11 ms) (2 patients). The section thickness was 2 mm (15 sections), with an intersection gap of 0.3 mm. The FOV was 125 mm with a matrix of 256 × 256, resulting in an in-plane resolution for conventional MR images of 0.49 × 0.49 mm^2. In addition, whole-brain postcontrast spin-echo T1-weighted images (section thickness, 5 mm) were obtained to check for midline abnormalities (trilateral retinoblastoma).

DWI

DWI acquisitions (TR, 1450 ms; TE, 115 ms) were performed in the transverse plane by using a HASTE sequence and b-values of 0 and 1000 s/mm^2. Diffusion-weighting pointed in the direction of the spatial diagonal. To obtain a sufficient signal–to-noise ratio, we obtained 5 $b=0$ acquisitions and 15 $b=1000$ acquisitions. FOV was 125 mm, and matrix size, 192 × 192 mm, resulting in an in-plane resolution for DWI of 0.65 × 0.65 mm^2. Again, the section thickness was 2 mm, with an intersection gap of 0.3 mm. The total DWI acquisition time for 15 sections was 7.5 minutes. Afterward, ADC maps were calculated on the scanner.

Image Analysis

Two reviewers evaluated conventional MR images in consensus. Reviewers were blinded to the results of histopathology. All intraocular lesions were characterized on the basis of SI on T1- and T2-weighted MR images and enhancement characteristics. Tumor-volume measurements were performed by 1 reviewer on contrast-enhanced axial T1-weighted images with the use of a computerized image-analysis tool that is available as part of the PACS of our hospital (Centricity Radiology RA 600; GE Healthcare, Milwaukee, Wisconsin). In all sections in which tumor was present, we manually outlined this structure and calculated the tumor volume, taking section thickness and gap into account.

Evaluation of DWI (ie, on the $b=1000$ images) included identification of intraocular lesions and scoring of SI (high, intermediate, low) compared with the vitreous. The delineation of lesions on ADC maps was performed by both reviewers. We assessed separate mean ADC values for enhancing tumor tissue (solid tumor part) and for nonenhancing tumor tissue (areas of suspected necrosis). Necrosis was suspected if that part of the tumor showed a relatively high SI on T2-weighted images, with corresponding areas of relatively scarce or no enhancement on contrast-enhanced images. Areas of suspected calcifications (spots of SI void were present on all conventional series) were excluded. The ADC value and SD were calculated by manually outlining the lesions by region of interest on the axial images that contained (enhancing or nonenhancing) tumor tissue. Regions of interest were defined as slightly smaller than the actual lesions to avoid partial volume effects. Region-of-interest size ranged from 49 to 1687 mm^3 for enhancing parts and from 83 to 699 mm^3 for nonenhancing parts. ADC values were compared with histopathologic results. Also we assessed the mean ADC values of the vitreous body and of subretinal fluid in eyes showing a retinal detachment on T2-weighted images.

Histopathologic Analysis

One pathologist, who was blinded to patient clinical records and MR imaging findings, evaluated histopathologic specimens of the enucleated eyes. All histopathologic specimens were cut parallel to the axial

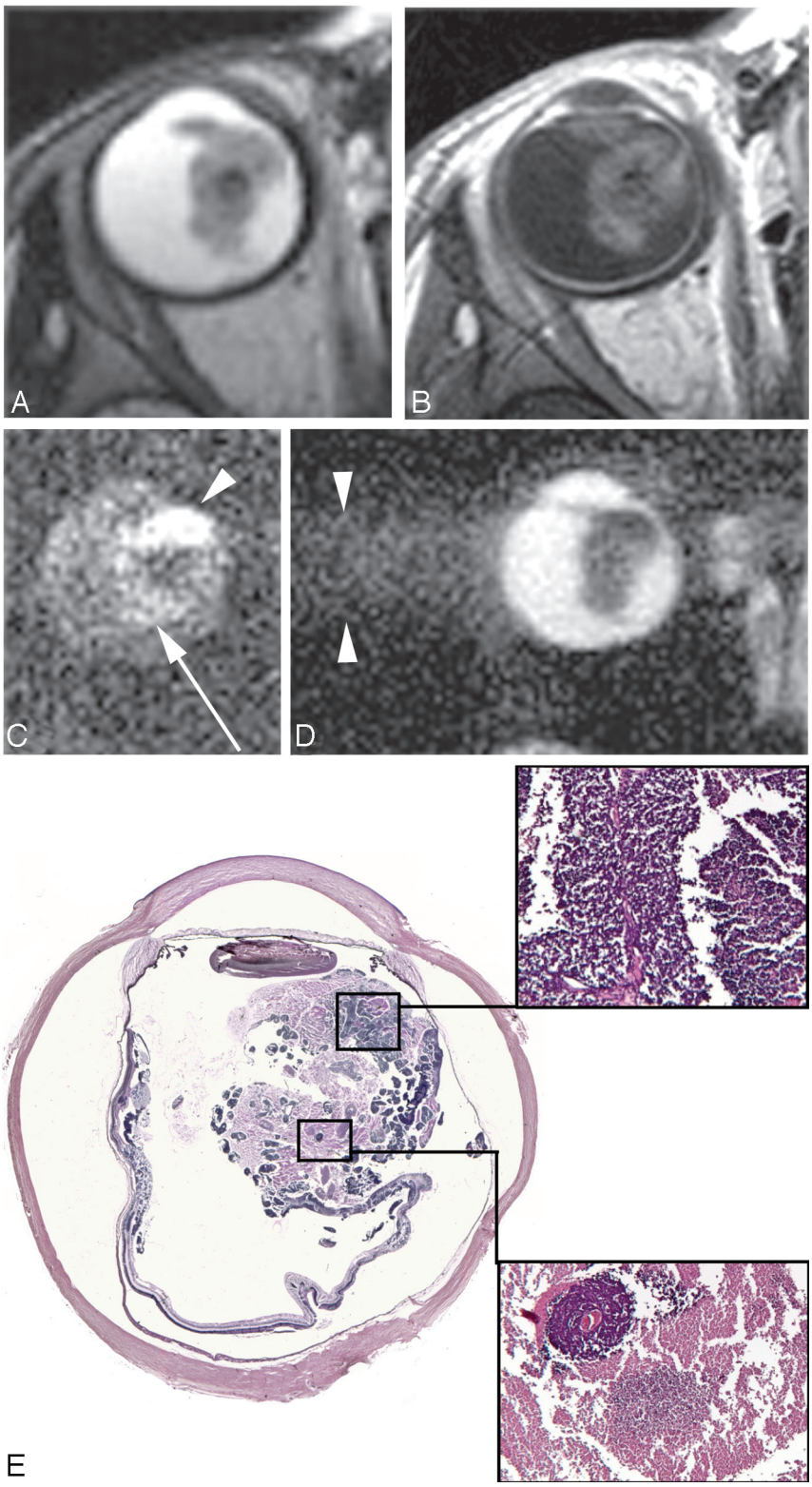

Fig 1. A 34-month-old girl with sporadic unilateral retinoblastoma of the right eye. *A* and *B*, Axial T2-weighted (*A*) and contrast-enhanced T1-weighted (*B*) MR images show an anteriorly located retinoblastoma with inhomogeneous SI. *C*, Axial DWI (b-value, 1000 s/mm^2) shows a markedly increased SI anteriorly in the mass on DWI (*arrowhead*) compared with the posterior part of the mass (*arrow*). *D*, On the ADC map, a reciprocal pattern is recognized with the lowest ADC values anterior in the tumor (mean ADC value, 1.09×10^{-3} mm^2/s). Axial ADC map shows linear blurring artifacts caused by the long echo train in the HASTE sequence. *E*, Histopathologic specimen shows poorly differentiated vital tumor tissue anteriorly (upper inset) and necrosis with some foci of vital tumor tissue posteriorly (lower inset) in the eye (H&E, original magnification ×3.5).

plane of the MR images in the presence of 1 of the MR image observers, to provide an optimal correlation between MR images and histology. Histopathologic evaluation, by using H&E staining, included the regional assessment of the degree of tumor differentiation (poor without rosettes, intermediate with spare rosettes, and well with many rosettes or photoreceptor differentiation) in viable tumor tissue. Top-

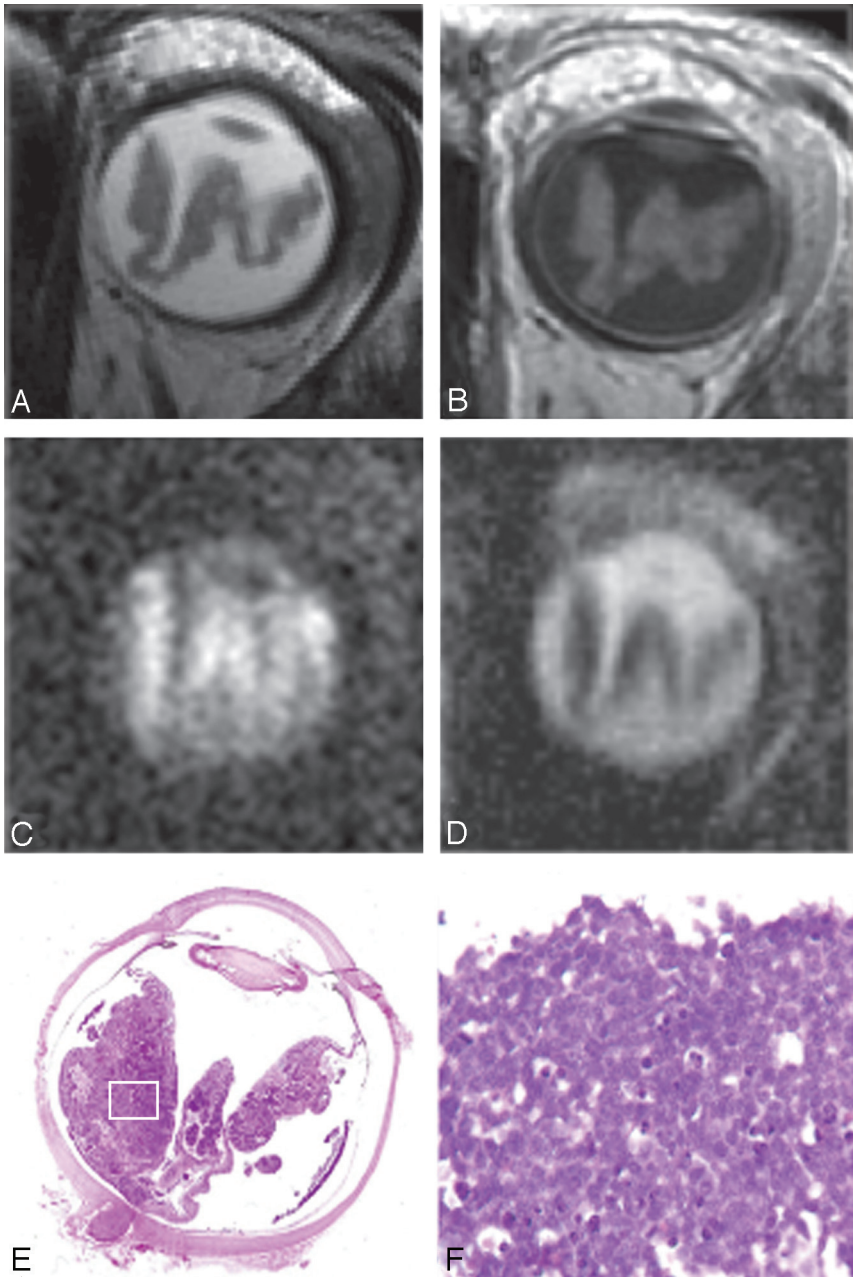

Fig 2. *A* and *B*, A 27-month-old boy with sporadic unilateral retinoblastoma of the left eye. Axial T2-weighted (*A*) and contrast-enhanced T1-weighted (*B*) MR images show a diffuse infiltrating retinoblastoma along the totally detached retina. *C* and *D*, On the axial DWI (b-value, 1000 s/mm^2) (*C*), the tumor shows diffuse hyperintense SI with a corresponding low ADC value (mean ADC value, 1.09 $\times$ 10^{-3} mm^2/s) (*D*). The mean ADC value of subretinal fluid is slightly lower compared with the remaining vitreous (1.99 versus 2.64 $\times$ 10^{-3} mm^2/s, respectively). *E*, Histopathologic specimen shows a totally detached retina, diffusely infiltrated by retinoblastoma (H&E, original magnification 3.5). Slightly more tumor tissue is present in the medial part of the eye on histopathology compared with the MR imaging because of a minor angulation within the cutting plane compared with the axial plane of the MR image. *F*, Inset: photomicrograph of the specimen shows poorly differentiated vital retinoblastoma, with densely packed cells (H&E, original magnification $\times$20).

ographic analysis of regions of viable tumor and necrosis was performed for regional correlation with ADC maps.

Statistical Analysis

All data were analyzed with the Statistical Package for the Social Sciences software package (SPSS for Windows, Version 15.0; SPSS, Chicago, Illinois). Linear mixed models with Bonferroni-corrected *P* values were used to assess pair-wise comparisons of quantitative MR imaging data (ADC values of the vitreous, subretinal fluid, and nonenhancing and enhancing tumor parts). For optimal model fit, a heterogeneous compound symmetry covariance matrix was used. Statistical significance was accepted with *P* values $<$ .05.

Results

Retinal detachment was observed on MR images in 15 of 17 eyes, of which 7 showed a total retinal detachment, obscuring the vitreous. Tumor seeding was clinically present in 6 eyes; 5 showed vitreous seeding and 1, subretinal seeding. Three patients showed a subretinal hemorrhage, including fluid-fluid layering in 2 of those. Mean tumor volume on MR images was 1520 mm^3 (range, 513-2721 mm^3).

DWI and ADC Maps

HASTE DWI (b=1000 images) and ADC maps were acceptable for interpretation in all patients. DWI enabled depiction

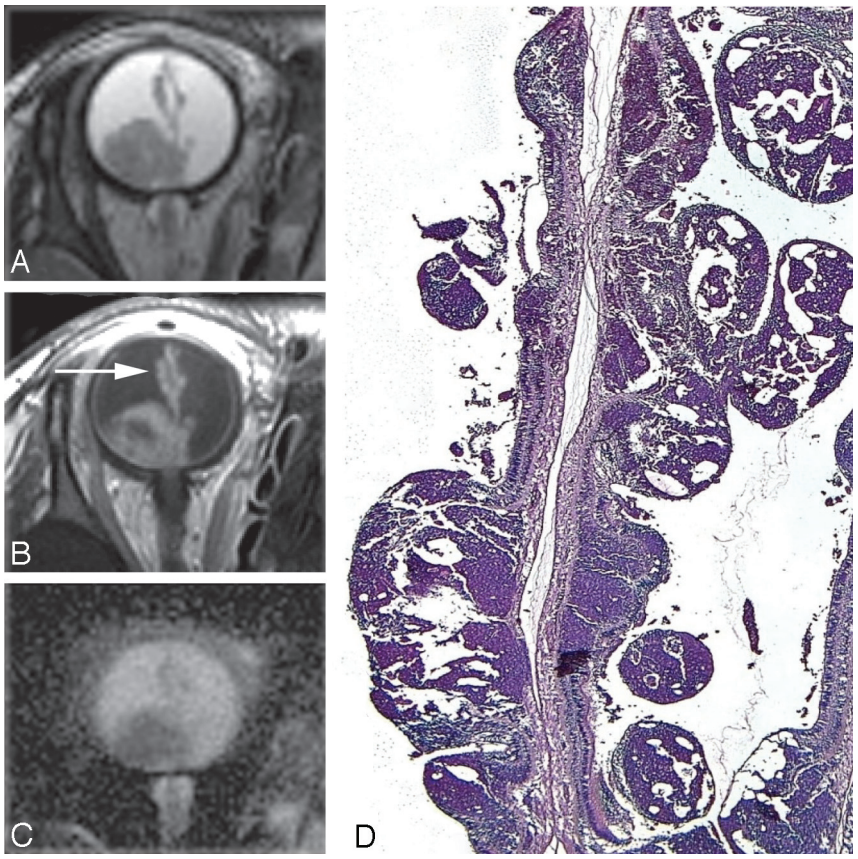

Fig 3. A 30-month-old girl with enucleation of the right eye because of sporadic bilateral retinoblastoma. *A–C*, Axial T2-weighted MR image (*A*), contrast-enhanced T1-weighted MR image (*B*), and ADC map (*C*) show multifocal retinoblastoma with a large subretinal mass (mean ADC value of the tumor mass, 1.03×10^{-3} mm^2/s; of the subretinal fluid, 2.35×10^{-3} mm^2/s) and multiple small nodules along the detached retina, which can also be encountered on the ADC map (too small for ADC measurement). *D*, Photomicrograph of a histopathologic specimen shows a multifocal poorly differentiated vital retinoblastoma, with multiple small noduli along the detached retina (H&E, original magnification ×3.5).

of the eyes in all included patients without any obvious image distortions (Figs 1 and 2). On the b=0 images (and consequently on the ADC maps [Fig 1*D*]), a blurring is observed due to the long echo train of the sequence. In all patients with newly diagnosed retinoblastoma, the delineation of the intraocular lesion was possible on DWI and ADC maps and was additionally confirmed on conventional T1- and T2-weighted MR images. Even small tumor nodules in the multifocal retinoblastoma can be depicted on ADC maps (Fig 3).

In general, DWI showed a high SI of retinoblastoma relative to the lower SI of the adjacent vitreous body or subretinal fluid (Fig 4). Typically, tumors showed an inhomogeneous pattern on DWI (high and intermediate SI regions) and ADC maps (low with intermediate ADC values). This pattern was comparable with the distribution of enhancing and nonenhancing lesions in the tumor on conventional MR images (Fig 1). Only 2 small tumor masses (tumor volumes of 513 and 611 mm^3) showed a homogeneous SI on DWI and ADC maps. In 1 patient, the tumor did not show enhancement and was suspected of being totally necrotic (Fig 5). The corresponding DWI showed no hyperintensity, and ADC values were intermediate. In 7 (41%) patients, the nonenhancing tumor parts were so small that reliable ADC measurements of these regions were not achieved. ADC values of the enhancing tumor parts were significantly lower compared with nonenhancing parts ($P < .0005$) (Table). In every single affected eye in which enhancing and nonenhancing tumor parts were measured, the mean ADC value of the nonenhancing tumor part was always higher than the mean ADC value of the enhancing part. There was only minor overlap in the range of ADC values between enhancing and nonenhancing tumor parts (Fig 6).

In 3 patients, subretinal fluid collections were too small for reliable ADC measurements. The mean ADC value of nonenhancing parts of the retinoblastoma was significantly lower than that of subretinal fluid ($P < .0005$) or surrounding vitreous ($P < .0005$) (Table and Fig 6). The difference in ADC values of subretinal hemorrhage compared with subretinal effusion was not statistically significant ($P = .55$) (Table). The difference between ADC of vitreous with or without tumor seeding was not statistically significant ($P = .39$) (Table).

ADC Maps Compared with Histopathologic Findings

ADC maps of individual patients were compared with histopathologic sections after enucleation to explain regional differences within tumors on ADC maps. These differences in ADCs reflect distinct differences in the histopathologic features of retinoblastoma (Figs 1, 2, and 4). Areas with low SI on ADC maps correlated to viable tumor tissue on histopathology, in which tumor parts showed the densest cellular packing (hypercellularity) (Figs 1, 2, and 4). Areas with intermediate SI on ADC maps correlated to (hypocellular) necrotic tumor tissue (Fig 1). In 1 patient, the tumor was totally necrotic, showing an intermediate SI on ADC maps throughout the tumor (Fig 5).

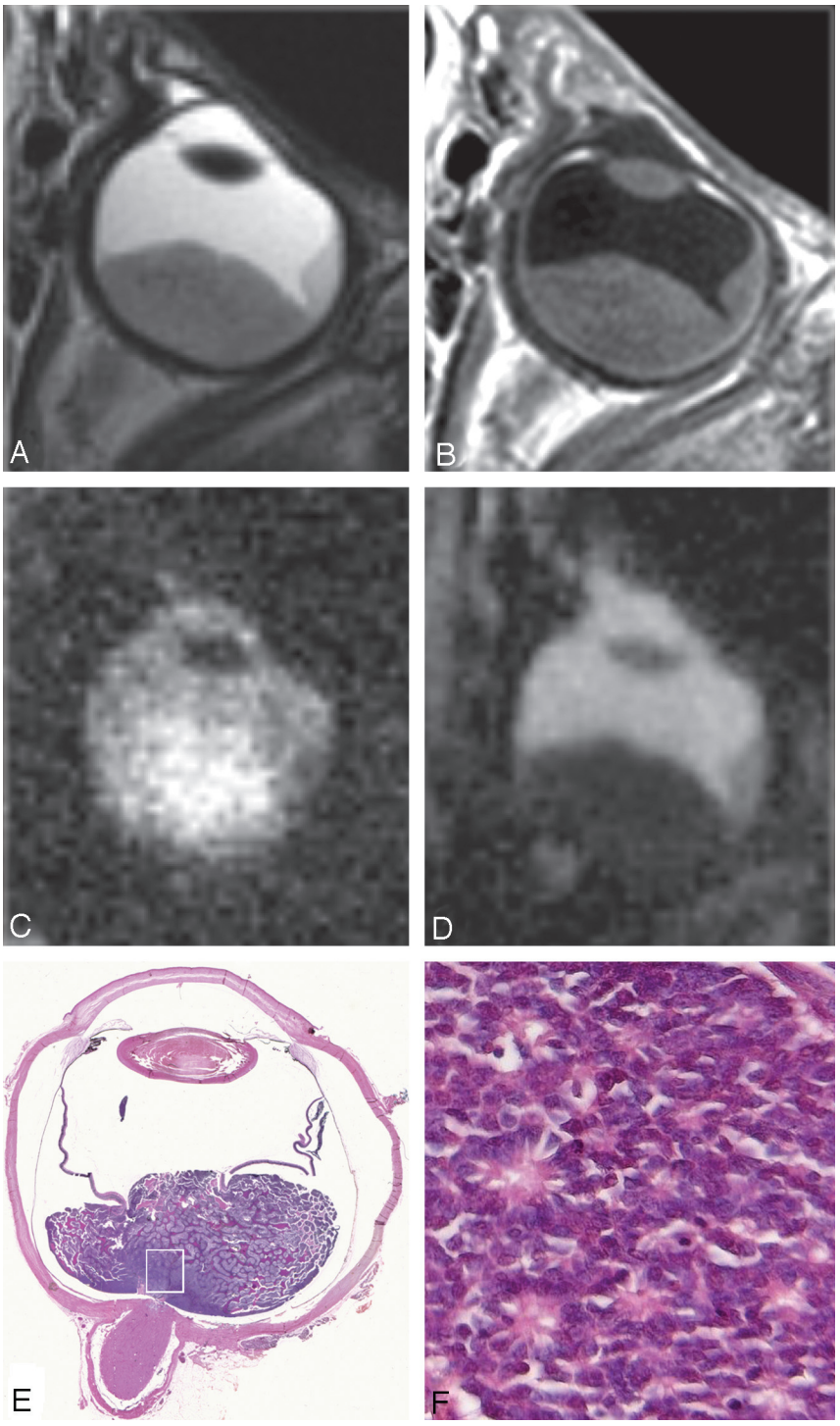

Fig 4. A 9-month-old boy with sporadic unilateral retinoblastoma of the left eye. *A* and *B*, Axial T2-weighted (*A*) and contrast-enhanced T1-weighted (*B*) MR images show a relatively homogeneous tumor mass combined with retinal detachment, compatible with retinoblastoma. *C* and *D*, On axial DWI (b-value, 1000 s/mm^2) (*C*), the tumor shows diffuse hyperintense SI with corresponding low ADC values (mean ADC value, 0.82 × 10^{-3} mm^2/s) (*D*). *E*, Histopathologic specimen shows a compact subretinal tumor mass located posteriorly in the eye combined with retinal detachment (H&E, original magnification × 3.5). *F*, Inset: photomicrograph of the specimen shows poorly differentiated vital retinoblastoma, with densely packed cells (H&E, original magnification ×20).

The degree of tumor differentiation in viable tumor tissue was as follows: 12 were poorly differentiated (Fig 2), 3 were intermediate with sparse rosette formation (Fig 4), and 2 were well-differentiated with many rosettes. There was no statistically significant difference between mean ADC values of poorly differentiated and intermediate or well-differentiated vital tumor tissue ($P = .97$).

Discussion

This study showed the feasibility of the application of HASTE DWI in the orbit. Our results demonstrate the potential value of this technique in the evaluation of retinoblastoma. Because diffusion restriction was consistently present in retinoblastoma, this imaging feature may be helpful in the characterization of intraocular lesions in children presenting with leuko-

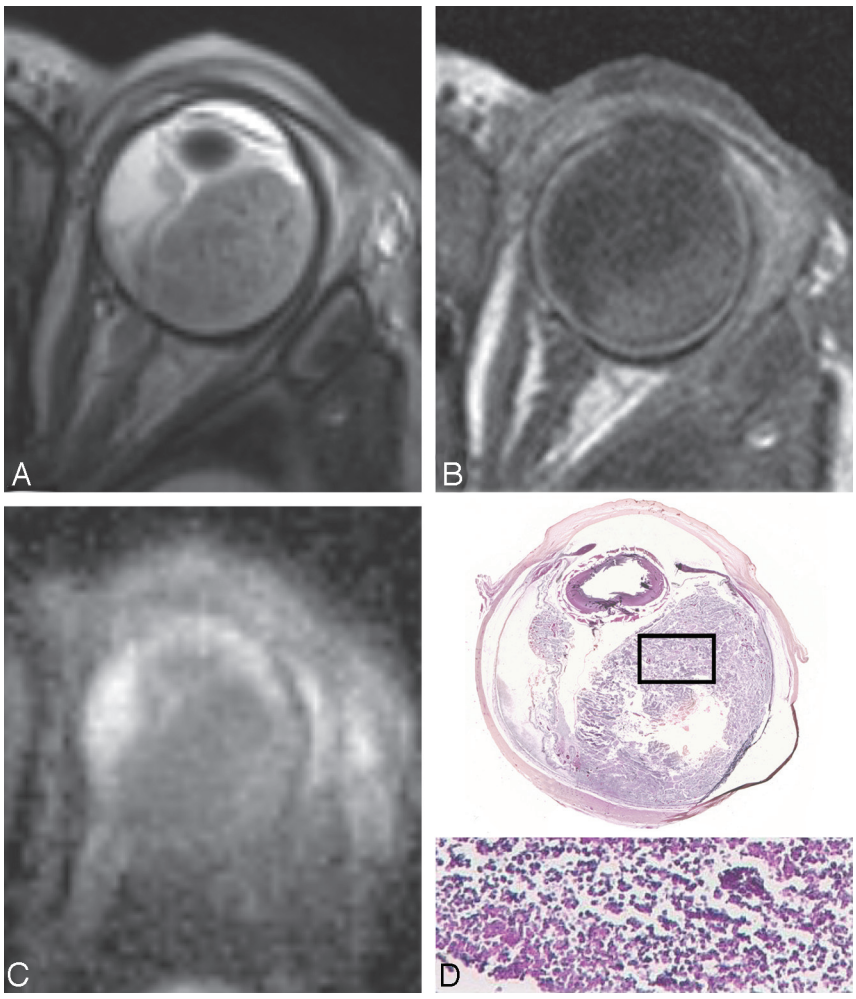

Fig 5. A 1-month-old girl with sporadic unilateral retinoblastoma of the left eye, who presented with orbital cellulitis and uveitis secondary to necrotic multifocal retinoblastoma. *A,* Total retinal detachment with a large subretinal mass temporal in the eye with low SI on a T2-weighted MR image, in combination with lens luxation and inflammatory changes in the preseptal soft tissues. *B,* The contrast-enhanced T1-weighted MR image shows absence of enhancement of the retinoblastoma; high SI posterior and temporal in the eye is also present on the precontrast T1-weighted image (not shown) and is suspicious for (hemorrhagic) necrosis. Note strong enhancement of the choroid with absence of iris enhancement. *C,* ADC map shows intermediate SI throughout the tumor (mean ADC values, tumor 1.73 × 10^{-3} mm^2/s). *D,* Histopathologic specimen shows multifocal retinoblastoma with a large friable subretinal mass (H&E, original magnification × 3.5). Inset: photomicrograph of the specimen shows details of necrotic tumor cells with loss of cell cohesion (H&E, original magnification, ×3.5).

Mean of ADC values for retinoblastoma, subretinal fluid, and vitreous

Parameter	ADC Value	Range
Retinoblastoma		
Enhancing tumor part	1.03 ± 0.15	0.72–1.22
Nonenhancing tumor part	1.47 ± 0.27	0.99–1.80
Subretinal fluid	2.20 ± 0.37	1.76–2.97
Hemorrhage	2.08 ± 0.22	
Effusion	2.24 ± 0.19	
Vitreous	2.67 ± 0.28	2.24–3.20
With tumor seeding	2.58 ± 0.21	
Without tumor seeding	2.75 ± 0.33	

coria—for the diagnosis of solid intraocular masses in particular. In this study, the ADC value differed significantly between the viable and necrotic parts of the tumor.

Regarding DWI techniques in the orbit, the advantage of the distortion-free HASTE sequence is that the DWI and ADC maps obtained with this technique can be reliably coregistered with high-resolution conventional MR images. However, the HASTE sequence has a lower signal–to-noise ratio than the commonly used EP sequences, but this was partly compensated for by obtaining multiple averages, which is especially needed with the currently used spatial resolution. The reduced sensitivity to susceptibility artifacts of HASTE DWI is especially important in retinoblastoma, because this tumor usually contains multiple foci of calcifications and the mean tumor volume in retinoblastoma is usually small (approximately 1 cm^3) compared with other primary tumors in the head and neck (approximately 7–10 cm^3).[17-19] By using a relatively high spatial resolution, even small intraocular lesions could be detected on ADC maps.

Restricted diffusion is a consistent imaging finding in vital retinoblastoma, demonstrating a high SI on DWI obtained at a high b-value and low SI on ADC maps. The appearance of this tumor on ADC maps can be explained by its histologic architecture. Generally, retinoblastomas have enlarged nuclei with scant cytoplasm and hyperchromatism, and they show hypercellularity. These histopathologic characteristics reduce the extracellular matrix and the diffusion space of water protons in the extracellular and intracellular dimensions, with a resultant decrease in the ADCs.[20] Comparing ADC maps with his-

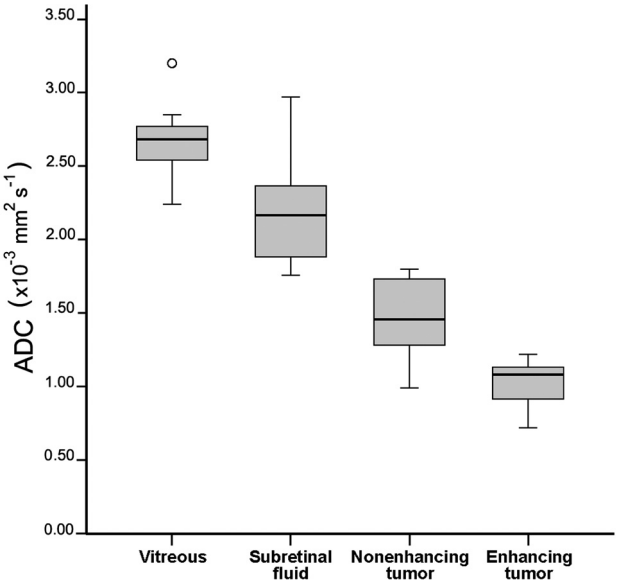

Fig 6. Box-and-whisker plots show the results for ADCs of the vitreous, subretinal fluid, and nonenhancing and enhancing tumor parts. There is hardly any overlap in the range of ADC values between enhancing and nonenhancing tumor parts of the affected eyes or between nonenhancing tumor parts and vitreous or subretinal fluid. The center line indicates the median; the bottom and top of the box, 25th and 75th percentiles respectively; *o*, outlier.

topathologic sections proved that differences in diffusion restriction between or even within tumors could be explained by regional differences in cellularity.

Viable tumor cells with intact membranes restrict water diffusion, whereas necrotic tumors have disrupted membranes, resulting in increased water diffusion.[21] In the context of a partially necrotic tumor, which is a very common finding in retinoblastoma, the region of necrosis would be expected to demonstrate a higher ADC value (less impeded diffusion) than would the vital portion; therefore, a region of necrosis would result in heterogeneity of the SI of retinoblastoma on DWI. In the present study, ADC values in necrotic tumor tissue were significantly higher than those in vital tumor tissue, with only minimal overlap of the ranges of ADC values. Because the results of our study show differences in ADC values between vital tumor tissue and necrosis, HASTE DWI may be an appropriate tool in the future for monitoring the effects of treatment in vivo or possibly pretreatment prediction of treatment outcome.

Poorly differentiated tumors are composed of densely packed cells in a random distribution. Tumor cells in highly differentiated retinoblastoma are clustered in a characteristic pattern, called Flexner-Wintersteiner rosettes.[22] An increasing number of rosettes are seen in highly differentiated tumors, with photoreceptor differentiation being the most advanced degree of retinal differentiation found in retinoblastoma (retinocytoma).[23] Highly differentiated tumors, with numerous rosettes and photoreceptor cell differentiation, display a relatively paucicellular cytoarchitecture with respect to poorly differentiated tumors. Therefore, we hypothesized that vital parts of highly differentiated tumors would show higher ADCs compared with poorly differentiated tumors; however, this hypothesis could not be confirmed by our analyses, possibly due to the small number of patients with intermediate or highly differentiated tumors.

The contrast of DWI is made up of the result of diffusion and T2 relaxation. Although vitreous has high SI on the $b=0$ image (due to its long T2 value), hardly any SI remains in the DWI, as long as the diffusion-weighting is strong enough (eg, with $b=1000$ s/mm^2). With this b-value, retinoblastoma showed good contrast of the lesion compared with the vitreous. In the DWI, additional anatomic information is lost, and conventional MR images are needed for detection of tumor extent. Obviously, the mean ADC of vitreous was markedly higher than that of vital or even necrotic retinoblastoma, because the mobility of water protons is higher in fluid than in tissues. The mean ADC value of vitreous ($2.67 \pm 0.28 \times 10^{-3}$ mm^2 s^{-1}) was slightly lower compared with a recently published ADC value ($3.06 \pm 0.12 \times 10^{-3}$ mm^2 s^{-1}).[13] However, such a small discrepancy can be expected due to differences in b-value ($b=700$ versus $b=1000$), in pulse sequence (EP versus non-EP DWI), and in voxel size (13 mm^3 versus 0.85 mm^3). The differences in ADC values between vitreous and subretinal fluid that we observed may be explained by the varying protein concentration of the subretinal fluid. The higher protein content in the latter will increase the viscosity and decrease the water proton mobility. The ADC of vitreous with tumor seeding, a clinically important prognostic factor for eye salvage, did show lower values compared with the normal vitreous; however, this difference did not reach a statistically significant difference, probably due to the small number of patients with seeding.

There are several limitations of the present study, which future studies can address. First, the sample size was too small to allow us to draw valid inferences on the possible influence of the degree of tumor differentiation on ADC values. The difference in ADC values between these tumor differentiation subgroups is probably quite small, which makes our preliminary study underpowered to find any difference. Second, in our study, we used 2 *b*-values for ADC calculations: 0 and 1000 s/mm^2. The b-value of 1000 s/mm^2 was chosen because the vitreous was nicely suppressed on these images. However, we did not investigate the possible influence of other b-values on the ADC of retinoblastoma[24] but used a constant value instead.

Conclusions

Non-EP DWI enabled adequate characterization of retinoblastoma, and ADC is a helpful tool to differentiate viable and necrotic tumor tissue. Therefore, HASTE DWI could be essential in possible future applications of this technique in the early prediction of response to eye-preserving therapies.

References

1. de Graaf P, Barkhof F, Moll AC, et al. **Retinoblastoma: MR imaging parameters in detection of tumor extent.** *Radiology* 2005;235:197–207
2. Brisse HJ, Guesmi M, Aerts I, et al. **Relevance of CT and MRI in retinoblastoma for the diagnosis of postlaminar invasion with normal-size optic nerve: a retrospective study of 150 patients with histological comparison.** *Pediatr Radiol* 2007;37:649–56
3. Lemke AJ, Kazi I, Mergner U, et al. **Retinoblastoma: MR appearance using a surface coil in comparison with histopathological results.** *Eur Radiol* 2007;17:49–60
4. Apushkin MA, Apushkin MA, Shapiro MJ, et al. **Retinoblastoma and simulating lesions: role of imaging.** *Neuroimaging Clin N Am* 2005;15:49–67
5. Vahedi A, Lumbroso-Le Rouic L, Levy Gabriel C, et al. **Differential diagnosis of retinoblastoma: a retrospective study of 486 cases.** *J Fr Ophtalmol* 2008;31:165–72

6. Muir KW, Buchan A, von Kummer R, et al. **Imaging of acute stroke.** *Lancet Neurol* 2006;5:755–68
7. Holodny AI, Makeyev S, Beattie BJ, et al. **Apparent diffusion coefficient of glial neoplasms: correlation with fluorodeoxyglucose-positron-emission tomography and gadolinium-enhanced MR imaging.** *AJNR Am J Neuroradiol* 2010; 31:1042–48
8. Kim S, Loevner L, Quon H, et al. **Diffusion-weighted magnetic resonance imaging for predicting and detecting early response to chemoradiation therapy of squamous cell carcinomas of the head and neck.** *Clin Cancer Res* 2009;15: 986–94
9. Hamstra DA, Galban CJ, Meyer CR, et al. **Functional diffusion map as an early imaging biomarker for high-grade glioma: correlation with conventional radiologic response and overall survival.** *J Clin Oncol* 2008;26:3387–94
10. Vandecaveye V, Dirix P, De Keyzer F, et al. **Predictive value of diffusion-weighted magnetic resonance imaging during chemoradiotherapy for head and neck squamous cell carcinoma.** *Eur Radiol* 2010;20:1703–14
11. Kapur R, Sepahdari AR, Mafee MF, et al. **MR imaging of orbital inflammatory syndrome, orbital cellulitis, and orbital lymphoid lesions: the role of diffusion-weighted imaging.** *AJNR Am J Neuroradiol* 2009;30:64–70
12. Sepahdari AR, Aakalu VK, Setabutr P, et al. **Indeterminate orbital masses: restricted diffusion at MR imaging with echo-planar diffusion-weighted imaging predicts malignancy.** *Radiology* 2010;256:554–64
13. Politi LS, Forghani R, Godi C, et al. **Ocular adnexal lymphoma: diffusion-weighted MR imaging for differential diagnosis and therapeutic monitoring.** *Radiology* 2010;256:565–74
14. Sepahdari AR, Aakalu VK, Kapur R, et al. **MRI of orbital cellulitis and orbital abscess: the role of diffusion-weighted imaging.** *AJR Am J Roentgenol* 2009;193: W244–50
15. Lovblad KO, Jakob PM, Chen Q, et al. **Turbo spin-echo diffusion-weighted MR of ischemic stroke.** *AJNR Am J Neuroradiol* 1998;19:201–08
16. de Foer B, Vercruysse JP, Bernaerts A, et al. **Middle ear cholesteatoma: non-echo-planar diffusion-weighted MR imaging versus delayed gadolinium-enhanced T1-weighted MR imaging—value in detection.** *Radiology* 2010;255: 866–72
17. de Graaf P, Knol DL, Moll AC, et al. **Eye size in retinoblastoma: MR imaging measurements in normal and affected eyes.** *Radiology* 2007;244:273–80
18. Ljumanovic R, Pouwels PJ, Langendijk JA, et al. **Has the degree of contrast enhancement with MR imaging in laryngeal carcinoma added value to anatomic parameters regarding prediction of response to radiation therapy?** *AJNR Am J Neuroradiol* 2007;28:1540–46
19. Ljumanovic R, Langendijk JA, Schenk B, et al. **Supraglottic carcinoma treated with curative radiation therapy: identification of prognostic groups with MR imaging.** *Radiology* 2004;232:440–48
20. Wang J, Takashima S, Takayama F, et al. **Head and neck lesions: characterization with diffusion-weighted echo-planar MR imaging.** *Radiology* 2001;220: 621–30
21. Seierstad T, Roe K, Olsen DR. **Noninvasive monitoring of radiation-induced treatment response using proton magnetic resonance spectroscopy and diffusion-weighted magnetic resonance imaging in a colorectal tumor model.** *Radiother Oncol* 2007;85:187–94
22. Wippold FJ, Perry A. **Neuropathology for the neuroradiologist: rosettes and pseudorosettes.** *AJNR Am J Neuroradiol* 2006;27:488–92
23. Eagle RC Jr. **High-risk features and tumor differentiation in retinoblastoma: a retrospective histopathologic study.** *Arch Pathol Lab Med* 2009;133:1203–09
24. Bogner W, Gruber S, Pinker K, et al. **Diffusion-weighted MR for differentiation of breast lesions at 3.0 T: how does selection of diffusion protocols affect diagnosis?** *Radiology* 2009;253:341–51